

# INFLUENCE OF SIMULTANEOUS CYCLIC LOADING AND EXTERNAL ALKALI SUPPLY ON THE ALKALI-SILICA REACTION IN CONCRETE PAVEMENTS

Frank Weise<sup>1</sup>, Katja Volland, Stephan Pirskawetz, Birgit Meng

BAM Federal Institute for Materials Research and Testing, Berlin, GERMANY

## Abstract

In recent years the German motorway network has seen an increase in the occurrence of damage to concrete road surfaces which can be attributed to the alkali-silica reaction (ASR). In view of the often drastically reduced life expectancy of road surfaces due to ASR, research activity in this field has notably increased. Alongside preventative measures in concrete technology, the main research focus up to now has been the development of performance-oriented testing procedures for ASR prevention. This included more specifically the accelerated simulation of climatic effects and external alkali penetration on road surfaces. The effects of mechanical pre-damage resulting from cyclic traffic loading and climatic impact had previously not been taken into consideration.

Since 2011, the five-partner research group 1498 sponsored by the German Research Foundation (DFG) has been pursuing research on how simultaneous cyclic loading and external alkali penetration impacts destructive ASR in road surface concretes. The depiction of the myriad degradation and transport processes necessary for an understanding of these effects requires close interaction between experiments and their multi-scale modelling. This paper aims to focus on the aforementioned experiments by means of innovative testing techniques. The research is founded on a series of cyclic fatigue tests performed on large-format beams, both with and without previous application of a sodium chloride (NaCl) solution, with simultaneous tracking of crack development. Subsequently, smaller test specimens were extracted from the pre-damaged beams for further experiments. These included the spatial visualization and quantification of fatigue-induced cracks using micro X-ray 3D-computed tomography (3D-CT). Additionally, the effects of fatigue-induced cracks on alkali transport were investigated using Laser-Induced Breakdown Spectroscopy (LIBS). Subsequent storage of the small-format test specimens, with and without cyclic pre-damage, in an ASR-conducive environment then provided initial findings on the influence of fatigue-induced pre-damage on the ASR.

**Keywords:** alkali-silica reaction, ASR, pavement concretes, mechanical pre-damage, external alkali supply

## 1 INTRODUCTION

In recent years the German motorway network has seen an increase in the occurrence of damage to concrete road surfaces which can be attributed to the alkali-silica reaction (ASR). Often this resulted in a halving of the planned utilisation period of the concrete pavement. Against this background ASR performance test methods have been developed in Germany to assess the residual ASR damage potential of existing concrete pavements as well as the avoidance of ASR damage on new motorway sections. However, these tests do not take into account the effects of mechanical pre-damage resulting from cyclic traffic loading and climatic impact on ASR damage processes. It can be expected that the cyclic tensile bending stress of the concrete pavement induces cracks in the tensile-stressed concrete boundary zone. These probably lead to increased penetration of moisture and de-icing salt. It is assumed that this in turn leads to an increase in the ASR damage process. The ASR research group 1498 was founded in 2011 to verify this working hypothesis. The German Research Foundation (DFG) extended the funding period for further three years in 2015. The depiction of the myriad degradation and transport processes necessary for an understanding of these effects requires a close interaction between experiments and their multi-scale modelling. In the research consortium the experiments are carried out by the "Institute for Building Materials" of the Ruhr-University Bochum (RUB), the "F. A. Finger-Institute for Building Materials Science" of the Bauhaus-University Weimar (BUW) and the division "Building Materials" of Federal Institute for Materials Research and Testing

---

<sup>1</sup> Correspondence to: frank.weise@bam.de

(BAM). Based on the findings, multiscale modelling is carried out by the “Institute for Structural Mechanics” of the Ruhr-University Bochum and the “Materials Testing and Research Institute” of the Karlsruhe Institute of Technology (KIT). This paper presents the findings of the BAM’s experimentally-oriented subproject. The experiments are based on the analysis of pre-damaged ordinary concrete pavements by means of four point bending tests on large-format beams with simultaneous capture of condition and damage indicators. The fatigue-induced cracks are visualized and quantified within extracted drilling cores by 3D-CT using novel recording and evaluation techniques. Additionally, the penetration of de-icing salt solution associated with mechanical cyclic loading was analysed using LIBS. Subsequent storage of the small-format test specimens, with and without cyclic pre-damage, in an ASR-conducive environment then provided initial findings on the influence of fatigue-induced pre-damage on the ASR.

## 2 CONCRETE AND TEST DESCRIPTION

### 2.1 Concrete mix designs and specimen production

All experiments were carried out by the research group on uniform practice-oriented pavement concretes (A and C). The coarse aggregates in concrete type A consist exclusively of granodiorite chippings (2/8, 8/16, 16/22) from Lusatia. Pavement concretes consisting of this slowly reactive aggregate are known to show damage due to ASR [1]. For the concrete type C the 2/8 granodiorite fraction was substituted by gravel chippings (2/8) from Upper Rhine. Concrete pavements made from this coarse aggregate also exhibit ASR-induced damage [1]. Additionally sand (0/2) from Rhine was used as fine aggregate. A more detailed petrographic and mineralogical characterisation of the chosen aggregates and additional test results on their alkali reactivity are given in [2], which also gives the chemical composition and physical properties of the road cement used (CEM I 42.5 N (sd), Na<sub>2</sub>O<sub>eq</sub> 0,73 M.-%). A water-cement ratio of 0.42 was chosen for the present concrete. The application of a common air-entraining agent ensured an air content of 4.0-4.5 Vol.-%, as the standard requirement [3]. Both types of concrete were produced with and without NaCl-boosting to obtain different internal ASR damage potentials. Table 1 gives an overview of the composition of all concrete types used.

Five minutes after mixing the fresh concrete parameters were determined. At the same time, the following specimens were produced for each concrete batch:

- one large-format beam 27 x 50 x 200 cm<sup>3</sup>
- two slabs 15 x 60 x 60 cm<sup>3</sup> from which three prisms 15 x 15 x 60 cm<sup>3</sup> were extracted to determine the bending tensile strength according to DIN EN 12390-5 (basis for the definition of the upper tensile stress during cyclic four point bending test)

The parameters of the fresh and hardened concrete of each batch of large-format beams are given in table 2.

### 2.2 Test set-up for mechanical cyclic pre-damage with condition and damage monitoring

The large-format beams were intended to provide a representative section of a concrete pavement slab. After 56-day storage in plastic sheets these beams were subjected to mechanical cyclic pre-damage by means of a four point bending test with simultaneous capture of condition and damage indicators (Figure 1). A single-span beam on two bearing points with cantilevers on both sides was selected as a static system. The cyclic loading was carried out symmetrically in the edge region of the cantilevers, generating a constant bending tensile stress between the bearing points on the upper side of the beam which had a broom-finished surface. This enabled the investigation of how an applied test solution impacts on mass transport and concrete degradation during cyclic loading. The cyclic loading input followed a sine curve with a frequency of 7 Hz to decrease test duration. The maximum load amounted to 60 % of the bending tensile strength determined for similar stored prisms (table 3). For this maximum load it can be assumed that the frequency of 7 Hz doesn’t increase significantly the number of cycles to failure [4]. The maximum number of load cycles was set at 5 million with a stress range of 1 N/mm<sup>2</sup> and a minimum stress of 1.2 or 1.4 N/mm<sup>2</sup>. This load function was developed on the basis of realistic assumptions with regard to stresses on concrete pavements induced by traffic and climate [5].

Intermittent rest and load phases were implemented in the test regime to capture non-destructively the damage evolution of the tensioned concrete boundary zone during cyclic loading (Figure 2a). The *rest phases* took place before mechanical loading according to a defined number of load cycles; during the rest phases, ultrasonic time of flight in the boundary concrete zone was determined using the ultrasonic device UK 1401 by Acoustic Control Systems. This enables conclusions to be drawn about the integral crack formation processes which are located there.

Additionally, the strain on the upper and underside of the large-format beam and the acoustic emissions were captured on defined load increments during the measurement phase, which was arranged before each cycling loading phase in the *load cycles* (Figure 2b). Both measured parameters provide information about the concrete degradation process. They were measured by means of strain gauges and the AE-system AMSY-5 by Vallen GmbH. A more detailed description of the test methodology developed can be seen in [6].

### **2.3 Characterisation of cyclic pre-damaged concrete microstructure by means of 3D CT**

For the spatial characterization of the microstructure changes in concrete associated with the cyclic loading, drilling cores were taken from large-format beams with and without cyclic pre-damage. The specimens gained were investigated by X-ray 3D computed tomography. More detailed information can be obtained in [7, 8]. However, the conventional investigation of the drilling cores (diameter 50 mm respectively 30 mm) with the micro focus X-ray system did not permit the visualization of the fatigue-induced cracks. Therefore subsections of the whole CT-measurement volume were enlarged by “Region of Interest Technology” (ROI technology). The reconstruction software CERA from Siemens AG was used for this purpose. This improved the local resolution of the 30 mm-diameter drilling core to 8  $\mu\text{m}$ , permitting the detection of cracks with a width of 5  $\mu\text{m}$  (crack length bigger than 24  $\mu\text{m}$ ). The quantitative three dimensional crack evaluations of the data sets was carried out with an automatic crack detection system which was used to verify the number, position, width and orientation of the existing cracks. This software tool was developed with the collaboration of the Zuse Institute Berlin (ZIB) and BAM [9-11].

### **2.4 Analysis of de-icing salt penetration in concrete by means of LIBS**

The effects of the cyclic pre-damage of the pavement concrete on alkali and chlorine penetration were verified using LIBS [12-14]. This method has a higher sensitivity to sodium than micro X-ray fluorescence analysis ( $\mu\text{-XRF}$ ). The measuring principle is shown in figure 3: a pulsed, focussed laser beam is applied to the surface of the building material. The high power density of the laser beam leads to vaporisation of a small near-surface area, generating plasma. As it cools, the plasma decomposes and emits element-specific radiation. The spectroscopic analysis of the radiation enables the identification of the different elements. They can also be quantified by additional calibration. In the present case the distribution of sodium, chlorine and calcium in particular was analysed by LIBS in vertical cross sections of specimens subject to different loads. The determination of the calcium distribution is used to distinguish between the cement stone, which was of primary interest, and the aggregates. In this context it should be noted that the local resolution of LIBS is only sufficient to detect aggregates with a diameter bigger than 0.5 mm. In the present case, therefore, the amount of sodium and chlorine is related to the fine mortar content.

### **2.5 ASR-generating storage of concrete specimen using cyclic climate chamber test**

In order to verify the effects of the cyclic pre-damage of the pavement concrete on the ASR, six small-format prismatic samples were taken from each the large-format beams with and without cyclic pre-damage. All samples were located within the upper side of these beams between the two bearing points. The samples were then prepared and preconditioned, before being subjected to twelve cycles of climate change storage. Each cycle consists of three phases: four days drying, fourteen days fog storage and a three day freeze-thaw-cycle phase (see figure 4). After each drying phase the NaCl test solution (3.6 M-%) was applied to three specimens of each test series while demineralized water was applied to the other three. The linear expansion of the specimen which is determined after each freeze-thaw-cycle phase is used as a damage indicator. If the expansion exceeds a threshold of 0.5 mm/m or 0.4 mm/m (NaCl solution or water application) after twelve cycles, ASR damage potential is high. A detailed description of the test method is shown in [15].

## **3 RESULTS AND DISCUSSION**

### **3.1 Mechanical cyclic pre-damage of concrete with condition and damage monitoring**

In the rest phase, the change in the surface wave time of flight in the broom finished concrete boundary zone was shown to be the decisive damage indicator. As an example, figure 5 shows for three cyclic pre-damaged large-format beams that the relative dynamic modulus of elasticity gives a good depiction of the fatigue damage evolution in the maximally tensioned concrete boundary zone. Based on the chosen times of measurement, it can be seen that for all three mechanically pre-damaged large-format beams, the dynamic modulus of elasticity decreases most markedly at the beginning of the fatigue stress (up to 1 million sinusoidal loading cycles). During the following stable phase the

micro cracks grow continuously. The modulus of elasticity decreases at a significantly slower rate within this phase. The unstable phase, which occurred only for the broken beam C2-3-IV, could not be depicted due to the chosen time of measurement in this case. The smaller decrease of the relative dynamic modulus of elasticity of beam C1-3-I is caused by the low maximum stress during the load-function.

The strain measured during the loading cycles on the upper and underside of the large-format concrete beam and the acoustic emissions allow significantly better depiction of the temporal course of the pre-damage process. Taking the beams made from concrete type C2 (without applied NaCl solution) as an example, figure 6 shows the strain on the underside of the beam determined during each loading increment and the acoustic emissions occurring throughout the measurement phase, corresponding to the number of loading cycles. Both beams had by far the highest acoustic emission activity during the initial loading cycle. Twice as many events were recorded within beam C2-3-IV than in beam C2-2-IV. This is an indicator for the increased micro crack formation. As the cyclic loading (stable phase) proceeded, initial signs of an increased acoustic emission (instable phase) are recognizable exclusively for beam C2-3-IV after 3.1 million loading cycles. During the measurement phase of the 65th loading cycle (3.25 million sinusoidal loading cycles) a significant increase of the acoustic emissions is apparent. This was an indicator for the fatigue fracture which occurred within the next cyclic loading phase. The course of concrete degradation in the large-format beam as indirectly determined by acoustic emission analysis reflects the compressive strains on the underside of the beam measured during each loading increment in the measurement phase. It is noticeable for beam C2-3-IV that the strain value during the initial loading is elevated; these values clearly increased in each loading increment with the increasing number of load cycles. In this case there are also indications of the fatigue fracture from the 62nd loading cycle (after 3.1 million sinusoidal loading cycles). It is also remarkable that the compressive strain determined during the lowest load increment (beams C2-2-IV and C2-3-IV) only amounts to 90 or 80  $\mu\text{m}/\text{m}$  after 3.25 million or 5.0 million sinusoidal loading cycles. It can therefore be concluded that the micro cracks induced by mechanical pre-damage are very small. In this context the question arises if these cracks can be visualized using 3D-CT.

### **3.2 Characterisation of cyclic pre-damaged concrete microstructure by means of 3D-CT**

The capability of X-ray 3D-CT is demonstrated for example by using a drilling core (diameter: 30 mm) taken from the cyclic pre-damaged beam C2-3-IV. The vertical extraction of the drilling core was located 20 cm away from the fatigue fracture. Two different areas of the drilling core were investigated for comparison, one located in the tensioned boundary zone of the beam (maximum concrete degradation) and the other one in the middle of the beam (neutral axis, minimum degradation). The measurement arrangement is shown in figure 8a. At first an overview recording was conducted for each test area. Based on the results of the first tomography, specific areas (as shown in 7a) were selected and enlarged using ROI technology. This technology permits the detection of cracks with a width of 5  $\mu\text{m}$  (length  $\geq 24 \mu\text{m}$ ) within the chosen volume. Figure 7b compares the extracted cracks within the two ROI-volumes as 3-D isosurface images. It is noticeable that the concrete volume located in the tensioned boundary zone (maximum concrete degradation) exhibits a significantly higher crack density in comparison to the other volume. This result is confirmed by the statistical crack evaluation (Tab. 3). The whole volume of the cracks detected in the maximum degraded area is over twice as large as in the other area. This raises the question of what influence the fatigue-induced cracks have on mass transport.

### **3.3 Impact of cyclic pre-damage of concrete on de-icing salt penetration**

Figure 8 presents an example of the LIBS findings on the sodium and chlorine distribution in two vertical cross sections of the large-format beam (A1-1-IV) subject to different loads after cyclic loading with applied NaCl solution. Comparison of the area scans / depth profiles shows that a significantly higher sodium and chlorine penetration can be measured in the tensioned area of the concrete surface boundary zone. The chlorine penetration depth increases by 8 mm due to the pre-damage of the concrete. This trend is even greater for sodium. The maximum increase of the fine mortar-related sodium / chlorine content in the concrete surface boundary zone increases by 0.19 M.-% / 0.15 M.-%. This suggests that the cyclic opening and closing of the micro cracks leads to increased penetration of de-icing salt solution in the concrete. However, further experiments are required to provide statistical validation of this working hypothesis.

### 3.4 Impact of pre-damage of concrete on ASR

Figure 9 shows the results of the expansion measurements on small-format samples during the cyclic climate change storage. The specimens examined were taken from the beam C1-3-I (pre-damaged) and C1-4-I (without pre-damage). Although beam C1-3-I showed only moderate pre-damage (see Figure 5), the small-format specimens taken from this beam showed increased expansion regardless of the applied type of test solution from the start of the second test cycle. From the sixth test cycle onwards, the expansion of the small-format specimens covered with NaCl solution increased disproportionately. A possible explanation for this phenomenon is given by the sodium distribution in the vertical cross section of the specimens with and without cyclic pre-damage determined by LIBS after cyclic climate change storage. In figure 10 it can be seen that the basis value of the fine mortar-related sodium content of the pre-damaged concrete is nearly two times higher than the basis value of the concrete without pre-damage (0.32 to 0.17 M.-%). It can therefore be concluded that the sodium required for ASR to take place is available sooner and in higher quantities in pre-damaged concrete.

## 4 SUMMARY AND OUTLOOK

The findings gained during experiments carried out the DFG research group 1498 resulted in new knowledge in the following points:

- Provision of a novel test methodology for detailed depiction of fatigue-induced damage evolution in large-format beams made of concrete pavement subject to cyclic flexural tension
- Proof of the ability to visualize spatially and quantify fatigue-induced cracks in the tensioned concrete boundary zone using X-ray 3D-CT (novel recording techniques and image evaluation tools)
- Assumption of the generation of a “micro crack pump” in large-format beams subject to cyclic flexural tension with simultaneous application of a NaCl solution
- Evidence of the increase of ASR damage processes due to mechanical pre-damage of the concrete micro structure (increased penetration of de-icing salt and moisture in cyclic pre-damaged concrete during cyclic climate change storage)

On this basis the following investigations are planned for the second funding period:

- Expanding the test methodology described above to include Time Domain Reflectometry (TDR) for in-situ in-depth resolution moisture and salt measurement for fatigue tests with simultaneous application of a NaCl solution
- Testing, optimizing and applying 3D-CT for the in-situ analysis of moisture transport in small-format concrete cylinders with and without mechanical pre-damage as well as the characterization of ASR-induced cracks
- Deeper analysis of the influence of mechanically-induced pre-damage on the ASR by alternative ASR-conducive storage using different alkali reactive aggregates and cements with different Na<sub>2</sub>O equivalent

## ACKNOWLEDGEMENT

First of all the authors wish to thank the German Research Foundation for sponsoring this project. We also thank all partners of our DFG research group 1498 for the good cooperation. Furthermore we would like to say thank you to Dr. Med. K. Ehrig and Ing. D. Meinel (BAM) for carrying out and evaluating all measurements by  $\mu$ -3D-CT. Special thanks go also to Dipl.-Phys. G. Wilsch und M.Eng. Steven Millar (BAM) for the performance and evaluation of the measurement by LIBS.

## REFERENCES

- [1] Stark, J.; Freyburg, E.; Seyfarth, K.; Giebson, C.; Erfurt, D.: 70 Years of ASR with No End in Sight? ZKG International, No. 4-2010, pp.86-95(part 1) and No. 5-2010, pp. 55-70 (part 2).
- [2] Giebson, C.; Voland, K.; Ludwig, H.-M. und B. Meng: Untersuchungen zur Alkali-Kieselsäure-Reaktion in vorgeschädigten Fahrbahndeckenbetonen. In: Beton und Stahlbetonbau, 110 (2015), vol. 1, Ernst & Sohn, Berlin, pp. 13-21.
- [3] Forschungsgesellschaft für Straßen- und Verkehrswesen (FGSV): TL Beton-StB 07 – technische Lieferbedingungen für Baustoffe und Baustoffgemische für Tragschichten mit hydraulischen Bindemitteln und Fahrbahndecken aus Beton, 2007 edition.

- [4] Breitenbücher, R.; Kunz, S.: Influences of cyclic loadings on the properties of pavement concrete, ASCE Conference "Airfield and Highway Pavement", Los Angeles, 2013, Proceedings pp. 214 – 224.
- [5] Przondziona, R.; Timothy, J.; Nguyen, M.; Weise, F.; Breitenbücher, R.; Meschke, G. und B. Meng: Vorschädigungen in Beton infolge zyklischer Beanspruchungen und deren Auswirkung auf Transportprozesse im Hinblick auf eine schädigende AKR. In: Beton und Stahlbetonbau, 110 (2015), vol. 1, Ernst & Sohn, Berlin, pp. 3-12.
- [6] Weise, F.; Wiedmann, A.; Volland, K.; Kotan, E.; Ehrig, K. und H.S. Müller: Auswirkungen von Ermüdungsbeanspruchungen auf Struktur und Eigenschaften von Fahrbahndeckenbeton. In: Beton und Stahlbetonbau, 110 (2015), vol. 1, Ernst & Sohn, Berlin, pp. 22-33.
- [7] Weise, F.; Onel, Y. and F. Dehn: Application of X-ray tomography for the verification of damage mechanism in concrete. In: Proceedings of the International Conference on Concrete Repair, Rehabilitation and Retrofitting (ICRRR), Cape Town, South Africa, 21-23 November 2005.
- [8] Weise, F.; Pirskawetz, S.; Müller, U. und B. Meng: Charakterisierung der Schädigungsprozesse in Betonen mit innovativen Prüftechniken. In: Beton, 56 (2006), vol. 6, Verlag Bau + Technik, Erkrath, 2006.
- [9] Ehrig, K.; Goebbels, J.; Meinel, D.; Paetsch, O.; Prohaska, S. and V. Zobel: Comparison of crack detection methods for analyzing damage processes in concrete with computed tomography, DIR 2011 International symposium on digital industrial radiology and computed tomography, Proceedings, DGZfP-BB 128, pp. 1-8..
- [10] Paetsch, O.; Baum, D.; Ehrig, K.; Meinel, D. und S. Prohaska: Vergleich automatischer 3-D-Risserkennungsmethoden für die quantitative Analyse der Schadensentwicklung in Betonproben mit Computer Tomographie. DACH-Tagung 2012, DGZfP-BB 136, Graz, 2012.
- [11] Stalling, D.; Westerhoff, M. and H.-C. Hege: Amira: A Highly Interactive System for Visual Data Analysis. In C.D. Hansen, C. R. Johnson (eds.), The Visualization Handbook, Ch. 38, pp. 749-767, Elsevier, 2005.
- [12] Molkenhain, A.: Laser-induzierte Breakdown Spektroskopie (LIBS) zur hochauflösenden Analyse der Ionenverteilung in zementgebundenen Feststoffen. Dissertation, BAM-Dissertationsreihe, vol. 42, Berlin (2009).
- [13] Wilsch, G.; Eichler, T.; Millar, S. and D. Schaurich: Laser Induced Breakdown Spectroscopy (LIBS) - alternative to wet chemistry and micro-XRF. In: Proceedings of "1st International Conference on the Chemistry of Construction Materials", Berlin (2013).
- [14] Millar, S.; Wilsch, G.; Eichler, T.; Cassian, G. und H. Wiggerhauser: Laser Induced Breakdown Spectroscopy (LIBS) im Bauwesen – innovative Baustoffanalyse. In: Beton und Stahlbetonbau, 110 (2015), vol. 8, Ernst & Sohn, Berlin.
- [15] Stark, J. and K. Seyfarth: Assessment of specific pavement concrete mixture by using an ASR performance-test. In: Proceedings of the 12th ICAAR - International conference on alkali aggregate reaction, Trondheim, Norway, 15. - 18. June 2008.

TABLE 1: Composition of concrete.

Characteristic			Concrete type			
			A1	A2	C1	C2
type and fraction of aggregate	sand from Rhine 0/2		28		28	
	chippings of granodiorite 2/8		15		-	
	gravel chippings from Upper Rhine 2/8		-		15	
	chippings of granodiorite 8/16		27		27	
	chippings of granodiorite 16/22		30		30	
cement	type	CEM I 42,5 N (sd); [Na <sub>2</sub> O <sub>equ.</sub> : 0,73 M.-%]	X		X	
	content	[kg/m <sup>3</sup> ]	360		360	
w/c-ratio			0.42		0.42	
additive: LPS A 94 (0.2 M.-% related to cement content)			X		X	
boosting: 1.11 g NaCl/100 g cement			-	X	-	X

TABLE 2: Selected parameters of fresh and hardened concrete.

Parameter				Concrete batch of large-format beam				
				C2-2-IV	C2-3-IV	A1-1-IV	C1-3-I	C1-4-I
fresh	con-crete	air content	[Vol.-%]	4.5	4.7	4.5	4.7	5.0
		apparent density	[g/cm <sup>3</sup> ]	2360	2350	2360	2340	2320
hardened		bending tensile strength $f_{ct,fl}$ (56 day sheet storage)	[N/mm <sup>2</sup> ]	4.2 (0.12)	3.9 (0.21)	4,2 (0,18)	4.8 (0.2)	4.6 (0.19)

TABLE 3: Comparison of crack parameters in upper and middle ROI-volume of the drilling core taken from the pre-damaged beam C2-3-IV.

measuring volume	number of cracks	crack volume, total	average crack volume per crack
upper	3697	3,77 mm <sup>3</sup>	0,00102 mm <sup>3</sup>
middle	2026	1,51 mm <sup>3</sup>	0,000746 mm <sup>3</sup>

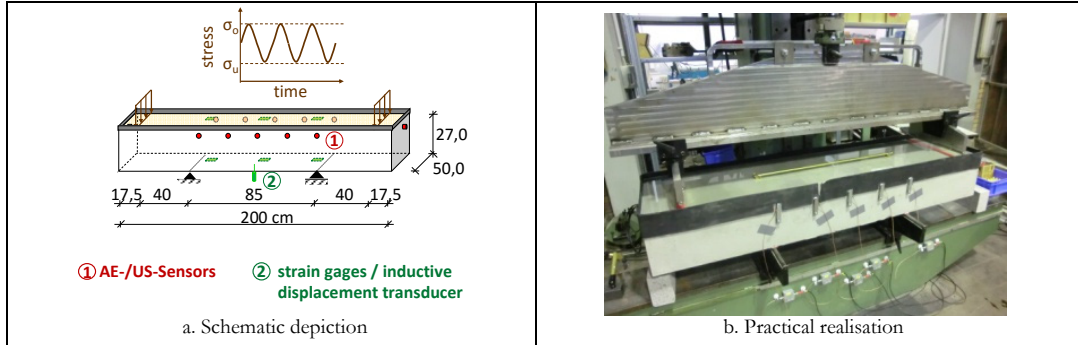


FIG. 1: Test set-up for the mechanical cyclic pre-damage of large-scale beams with penetration of NaCl-solution using a cyclic running four-point-bending test with condition and damage monitoring.

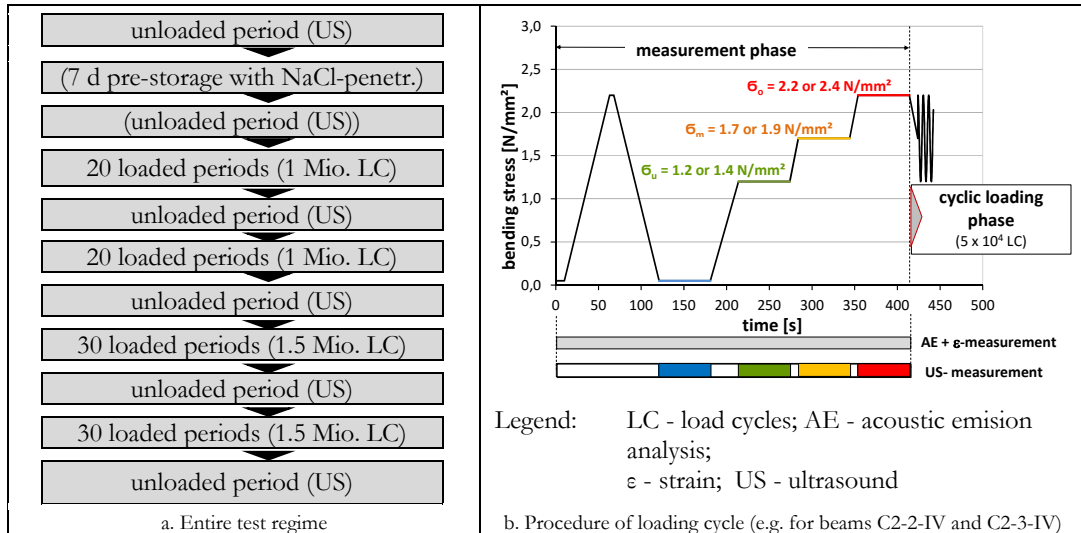


FIG. 2: Test regime of cyclic four-point-bending test of large-scale beams with additional monitoring of condition and damage indicators.

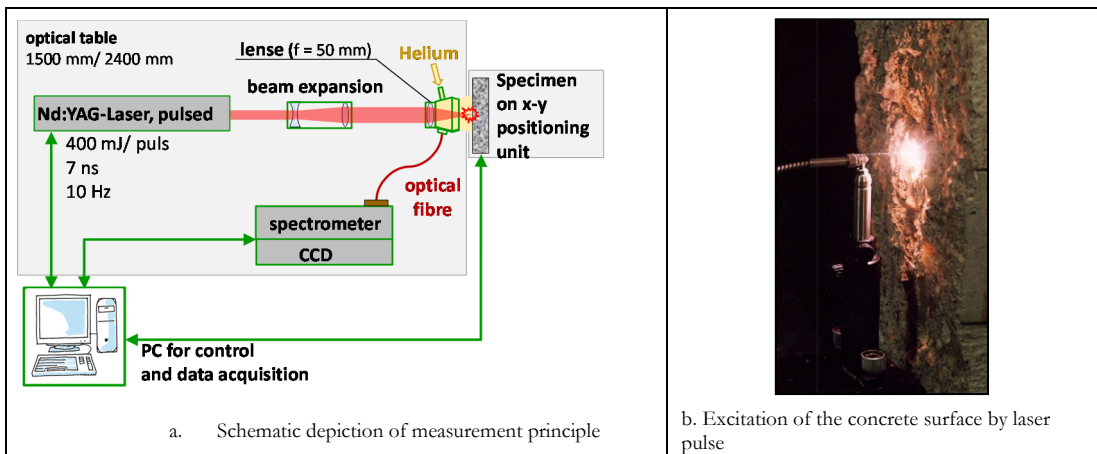


FIG 3: Measurement set-up of LIBS according to [14].

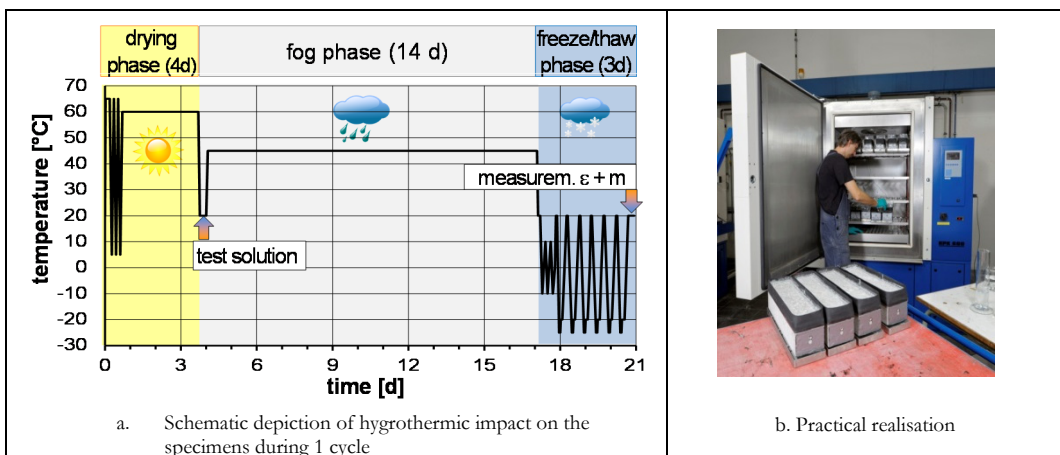


FIG 4: Description of the climate cyclic change storage.

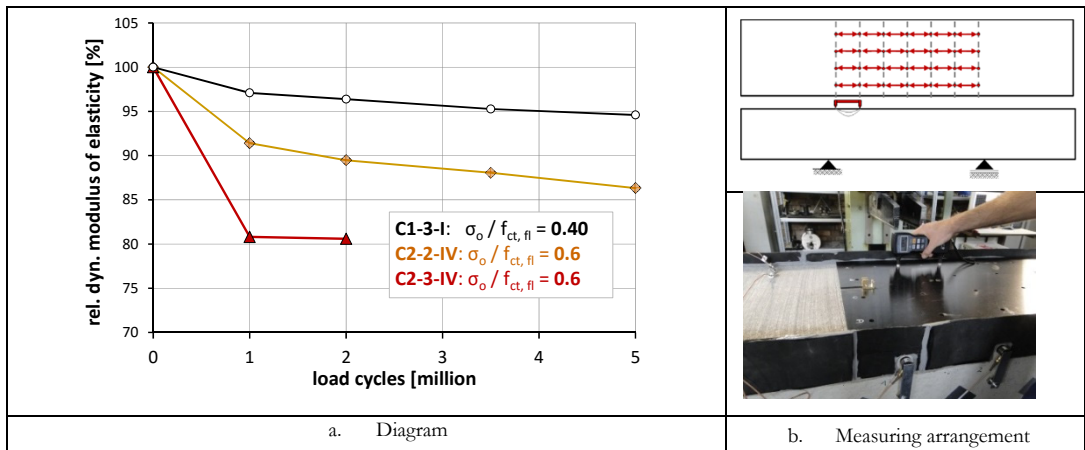


FIG.5: Comparison of mean values of dynamic modulus of elasticity determined by ultrasound measurement in concrete beams C1-3-I, C2-2-IV and C2-3-IV during the four-point-bending test without loading depending on cycle loading.

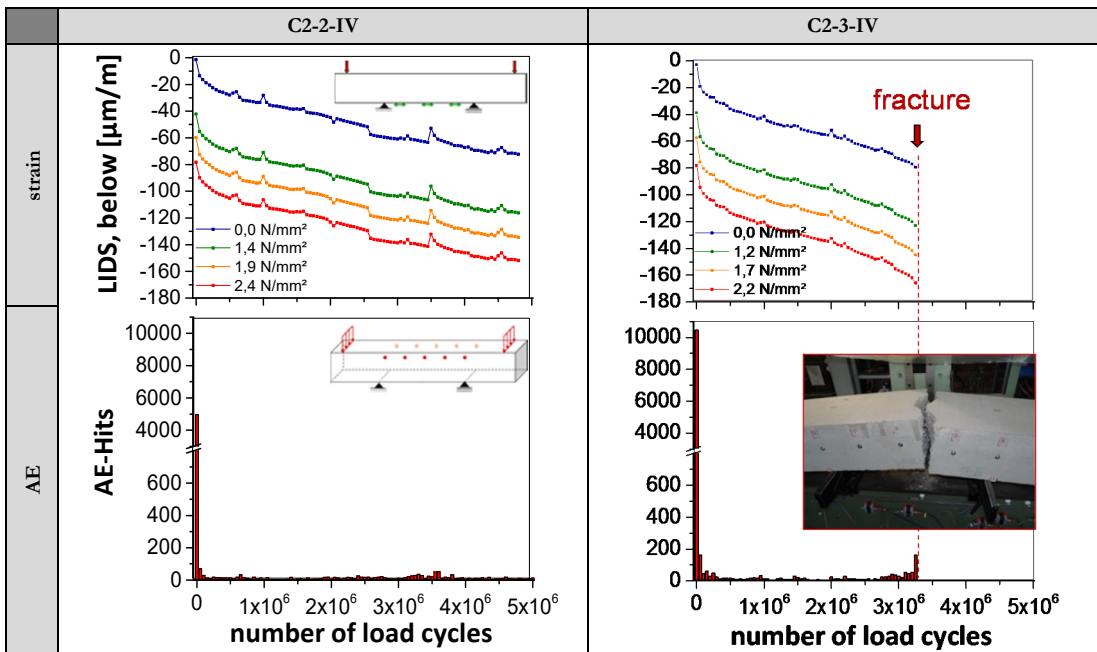
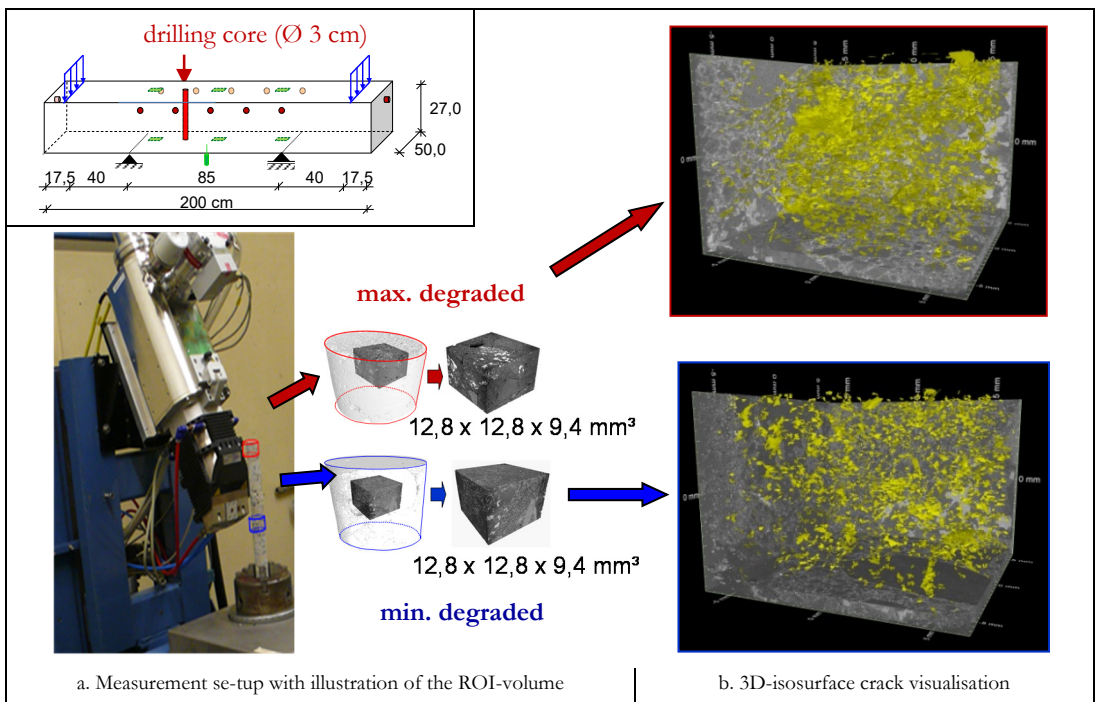


FIG. 6: Comparison of the temporal development of the underside strain and the acoustic emission activity determined under cyclic loading of beams C2-2-IV and C2-3-IV depending on the number of load cycles.



a. Measurement set-up with illustration of the ROI-volume

b. 3D-isosurface crack visualisation

FIG. 7: Characterisation of different degraded segments of a drilling core of the pre-damaged beam C2-3-IV (3.25 million load cycles) by X-ray 3D-CT.

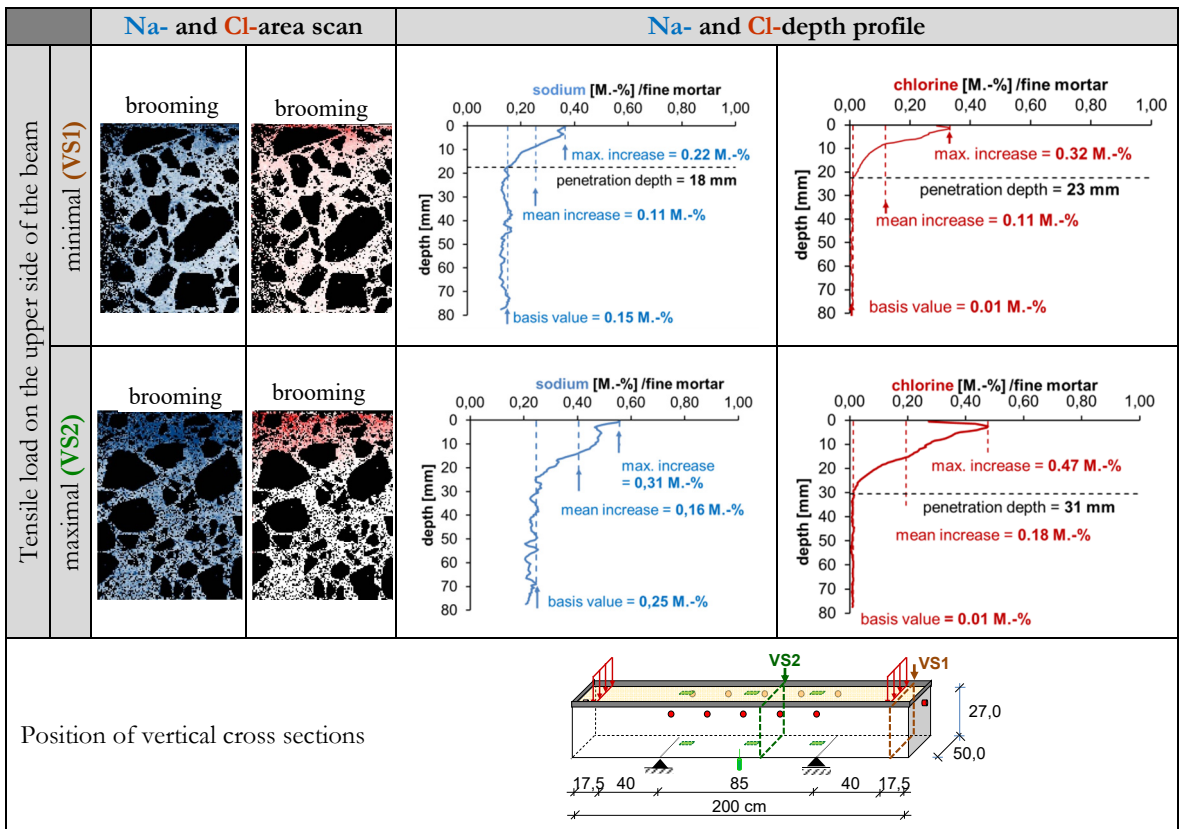


FIGURE 8: Na- and Cl-penetration in the boundary area of the beam A1-1-IV after cyclic loading with simultaneous penetration of test solution depending on concrete degradation.

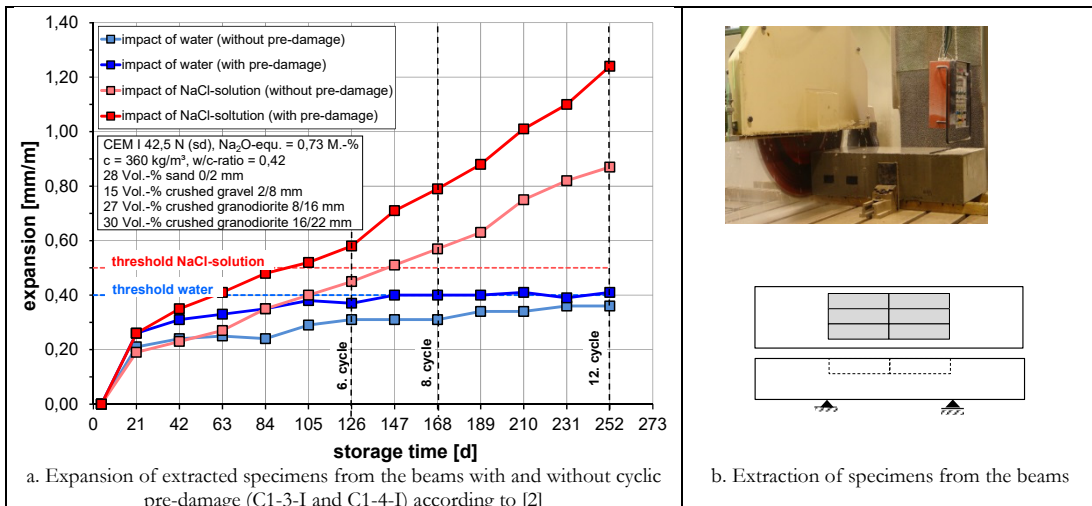


FIGURE 9: Results of cyclic climate change storage.

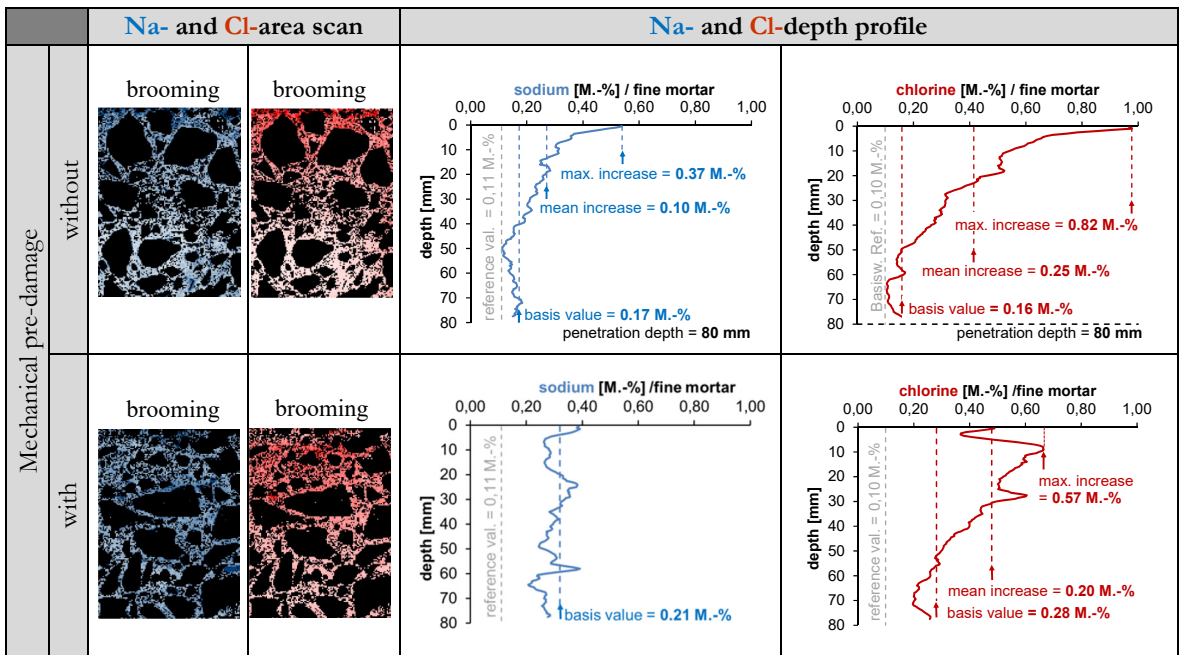


FIGURE 10: Na- and Cl-penetration in the small-format specimen of the beams C1-3-I and C1-4-I with /without mechanical pre-damage during the cyclic climate change storage (with simultaneous penetration of NaCl-solution).